The American Journal of Pathology, Vol. 192, No. 1, January 2022

The American Journal of
PATHOLOGY
ajp.amjpathol.org

See related Commentary on page 18

GASTROINTESTINAL, HEPATOBILIARY, AND PANCREATIC PATHOLOGY

METTL3 Regulates Liver Homeostasis, Hepatocyte Ploidy, and Circadian Rhythm—Controlled Gene Expression in Mice

Juan M. Barajas,* Cho-Hao Lin,*† Hui-Lung Sun,‡ Frances Alencastro,§ Allen C. Zhu,‡ Mona Aljuhani,* Ladan Navari,† Selen A. Yilmaz,¶ Lianbo Yu,¶ Kara Corps,‖ Chuan He,‡ Andrew W. Duncan,§ and Kalpana Ghoshal*†

From the Departments of Pathology, Biomedical Informatics,¶ and Veterinary Biosciences,‖ and the Comprehensive Cancer Center,† College of Medicine, The Ohio State University, Columbus, Ohio; the Department of Biochemistry and Molecular Biology and Institute for Biophysical Dynamics,‡ Howard Hughes Medical Institute, University of Chicago, Chicago, Illinois; and the Department of Pathology,§ Pittsburgh Liver Research Center, McGowan Institute for Regenerative Medicine, University of Pittsburgh, Pennsylvania*

Accepted for publication September 15, 2021.

Address correspondence to Andrew W. Duncan, Ph.D., Department of Pathology, McGowan Institute, PLRC, University of Pittsburgh, 450 Technology Dr., Ste 300, Pittsburgh, PA 15219; or Kalpana Ghoshal, Ph.D., Department of Pathology, The Ohio State University, 420 W. 12th Ave., Columbus, OH 43210. E-mail: duncana@pitt.edu or ghoshall@gmail.com.

N^6-methyladenosine (m^6A), the most abundant internal modifier of mRNAs installed by the methyltransferase 13 (METTL3) at the (G/A)(m^6A)C motif, plays a critical role in the regulation of gene expression. METTL3 is essential for embryonic development, and its dysregulation is linked to various diseases. However, the role of METTL3 in liver biology is largely unknown. In this study, METTL3 function was unraveled in mice depleted of *Mettl3* in neonatal livers (*Mettl3*$^{fl/fl}$; *Alb-Cre*). Liver-specific *Mettl3* knockout (M3LKO) mice exhibited global decrease in m^6A on polyadenylated RNAs and pathologic features associated with nonalcoholic fatty liver disease (eg, hepatocyte ballooning, ductular reaction, microsteatosis, pleomorphic nuclei, DNA damage, foci of altered hepatocytes, focal lobular and portal inflammation, and elevated serum alanine transaminase/alkaline phosphatase levels). *Mettl3*-depleted hepatocytes were highly proliferative, with decreased numbers of binucleate hepatocytes and increased nuclear polyploidy. M3LKO livers were characterized by reduced m^6A and expression of several key metabolic transcripts regulated by circadian rhythm and decreased nuclear protein levels of the core clock transcription factors BMAL1 and CLOCK. A significant decrease in total *Bmal1* and *Clock* mRNAs but an increase in their nuclear levels were observed in M3LKO livers, suggesting impaired nuclear export. Consistent with the phenotype, methylated (m^6A) RNA immunoprecipitation coupled with sequencing and RNA sequencing revealed transcriptome-wide loss of m^6A markers and alterations in abundance of mRNAs involved in metabolism in M3LKO. Collectively, METTL3 and m^6A modifications are critical regulators of liver homeostasis and function. *(Am J Pathol 2022, 192: 56—71; https://doi.org/10.1016/j.ajpath.2021.09.005)*

N^6-methyladenosine (m^6A) is the most prevalent internal modification in eukaryotic mRNAs identified to date.[1,2] m^6A is a chemical derivative of adenosine and is found at the consensus G[G>A]m^6**A**C[U>A>C] motif, usually concentrated at the 3′-UTR and the last exon.[3,4] m^6A is installed co-transcriptionally in the primary transcripts by the highly conserved methyltransferase 13 (METTL3)—methyltransferase 14 (METTL14) heterodimer, where METTL3 is the S-adenosylmethionine (AdoMet)-binding catalytic subunit and METTL14 facilitates substrate RNA binding.[5] Advancements in next-generation sequencing

Supported by NIH grants R01 CA193244 (K.G.), R01 DK103645 (A.W.D.), and RM1 HG008935 (C.H.); Comparative Pathology and Digital Imaging Shared Resource (CPDISR) and Genomics Shared Resource (GSR) of Ohio State University Comprehensive Cancer Center grant P30 CA016058; and Pittsburgh Liver Research Center Clinical Biospecimen Repository and Processing Core grant P30 DK120531.

A.W.D. and K.G contributed equally to this work as senior authors.

J.M.B., C.-H.L., and H.-L.S. contributed equally this work.

Disclosures: C.H. is a scientific founder and a scientific advisory board member of Accent Therapeutics Inc. and a Howard Hughes Medical Institute investigator.

Current address of J.M.B., Department of Oncology, St. Jude Children's Research Hospital, Memphis, TN.

https://doi.org/10.1016/j.ajpath.2021.09.005

technologies and detection methods for chemical modifications on RNA have allowed for rapid mapping and characterization of transcripts that harbor m^6A modifications.[6,7] These experiments have revealed an enrichment of m^6A sites in 3′-UTR regions near stop codons, 5′-UTRs, or terminal exon-exon junctions of mRNAs in thousands of transcripts in mice and humans.[4,6,7] AlkB homologue 5 (ALKBH5)[8] and fat mass and obesity-associated protein (FTO/ALKBH9)[9] are the two Fe^{2+}- and 2-oxoglutarate–dependent dioxygenases that demethylate m^6A. m^6A is recognized by members of the YT521-B homology (YTH-domain-containing protein) and the heterogeneous nuclear ribonucleoprotein proteins to modulate mRNA functions. Recent studies indicate that FTO preferentially demethylates m^6A_m in mRNAs and snRNAs and m^1A on tRNAs.[10,11] Notably, single-nucleotide polymorphisms within an intron of the *FTO* gene are associated with increased body mass index and the occurrence of obesity and diabetes in humans.[12]

m^6A marks regulate gene expression by influencing transcript stability, poly A site selection, processing, and translational efficiency.[13] Loss of m^6A in mouse and human embryonic stem cells (ESCs) blocked differentiation to different cell lineages without affecting their pluripotency.[14,15] Persistent expression of stem cell markers (eg, *Nanog*, *Oct4*) and lack of induction of lineage commitment genes (eg, *Brachyury*, *Foxa2*) are responsible for the observed phenotypes. Embryonic lethality of global liver-specific *Mettl3* knockout (M3LKO) mice revealed that m^6A is essential for mammalian development.[15] Although *Mettl3*$^{-/-}$ blastocysts appear normal, embryos exhibit deformities after implantation and are absorbed by embryonic day 8.5. Inability to turn off pluripotency genes and induce lineage commitment genes was also observed in M3LKO embryos. m^6A is critical for biological and physiologic processes, such as DNA damage repair[16] and circadian rhythms.[17] Aberrations in the m^6A profile have been linked to diseases and disorders, including cardiovascular disease,[18,19] metabolic disorders,[17] and cancer.[20] However, the alteration in molecular pathways and disease states resulting from aberrant m^6A landscapes is cell type specific and context dependent.[21] METTL3, METTL14, and FTO modulate tumorigenesis in a tissue-specific manner by regulating m^6A levels, which are dynamically regulated by stress and ionizing radiation.[16,22–24] Mutations in human genes encoding RNA modification enzymes, such as METTL3 and METTL14, have been linked to diseases such as cancer, cardiovascular and metabolic diseases, neurologic disorders, and mitochondria-related defects.[25,26] Recently, it was reported that m^6A modification is critical for suppressing endogenous retroviruses in mouse ESCs.[27,28] Silencing of endogenous retroviruses is essential for the maintenance of genomic integrity, the loss of which is associated with myriad diseases, including cancer and neurodegenerative disorders.

Mettl3 deletion in adult hepatocytes (using AAV8-TBG-Cre in *Mettl3*$^{fl/fl}$ mice) was recently reported to increase insulin sensitivity and reduce fatty acid synthesis in mice fed a high-fat diet, which correlated with decreased m^6A marks and expression of *Fasn*, indicating a role of METTL3 in fatty liver disease.[29] To investigate how METTL3 affects the liver in the absence of exogenous injury, M3LKO mice, in which *Mettl3* was deleted during neonatal development using *Alb-Cre*, were characterized.[30,31] The results indicate that METTL3 is critical for the maintenance of liver homeostasis because its lifelong depletion results in altered liver architecture, microsteatosis, development of polyploid hepatocytes, and proliferation of hepatocytes and bile duct cells. Molecular analysis revealed that METTL3 is critical for m^6A homeostasis in liver polyadenylated RNAs, hepatocyte maturation, and metabolic function. RNA sequencing analysis identified dysregulation of genes involved in metabolism, hepatic differentiation, and cell cycle control. Molecular analysis revealed that METTL3 is a master regulator of hepatic m^6A landscape and gene expression profile and is essential for hepatocyte maturation and metabolic function. Methylated (m^6A) RNA immunoprecipitation (meRIP) coupled with sequencing identified a large number of transcripts with m^6A marks, many of which are involved in metabolism and are targets of BMAL1 and CLOCK, key transcription factors involved in circadian rhythm control.[32] Thus, M3LKO mice provide a unique model to understand the functions of this important epitranscriptomic modification (m^6A) in liver biology and disease processes.

Materials and Methods

Generation of M3LKO Mice

M3LKO (*Mettl3*$^{fl/fl}$; *Alb-Cre*) mice were generated by crossing *Mettl3*$^{fl/fl}$ mice (provided by Dr. Jacob Hanna) with albumin-Cre mice (Jackson Laboratories, Bar Harbor, ME), and genotypes were confirmed by tail-DNA PCR using primers as previously described.[15] Animals were handled and euthanized following institutional guidelines. All animal studies were reviewed and approved by The Ohio State University Institutional Laboratory Animal Care and Use Committee.

Serum, Liver Histologic, and Immunohistochemical Analysis

Serum was collected from mice by cardiac puncture after CO_2 asphyxiation and cervical dislocation. Biochemical analysis of enzymes and lipids in the serum samples was performed at the Ohio State University Comparative Pathology and Mouse Phenotyping Shared Resource using VetAce (Alfa Wassermann System, West Caldwell, NJ).

For histologic analysis, a section of liver tissue was fixed in 4% paraformaldehyde and frozen in ornithine optimal

cutting temperature compound and/or embedded in paraffin. Hematoxylin and eosin (H&E) and Oil-Red-O staining of liver sections was performed as previously described.[33] H&E-stained slides were evaluated by a board-certified comparative veterinary pathologist (K.C.), with reporting of findings consistent with diagnostic and descriptive terms developed and approved by the International Harmonization of Nomenclature and Diagnostic Criteria Hepatobiliary Task Force in the Society of Toxicologic Pathology.[34] For immunohistochemical analysis, the slides were dewaxed and subjected to antigen retrieval at 95°C for 30 minutes, followed by incubation with the specific antibodies and color development by the DAB method and counterstaining with hematoxylin, and microscopic pictures were taken. The antibodies used for immunohistochemical analysis were ab195352 for METTL3 and ab273016 for WEE1 (Abcam, Cambridge, MA) and 14020 (for BMAL1), 12202 (for Ki-67), and 9718 for phospho-γ-H2a.x (Cell Signaling Technology, Danvers, MA). Immunohistochemical images were quantified using ImageJ software version 1.52a (NIH, Bethesda, MD; *http://imagej.nih.gov/ij*).

TUNEL Assay

Paraffin-embedded liver tissue sections were deparaffinized and incubated with 20 μg/mL of proteinase K for 30 minutes. The DeadEnd Colorimetric TUNEL System (G7360, Promega, Madison, WI) was used for terminal deoxynucleotidyl transferase-mediated dUTP nick-end labeling (TUNEL) staining according to the manufacturer's instructions.

Immunoblot Analysis of the Whole Liver Extracts and Liver Nuclear Extracts

Whole-liver lysates from snap-frozen liver tissues were prepared by suspension in radioimmunoprecipitation assay buffer (catalog number 9806; Cell Signaling Technology), followed by sonication to extract proteins and centrifugation at 4°C for 10 minutes to collect clear supernatants. Nuclear extracts were similarly prepared by extracting nuclear pellets as described for ploidy analysis.

Protein concentrations in the extracts were measured by the bicinchoninic acid method using bovine serum albumin as the standard. Equal amounts of protein from whole cell or tissue lysates were separated by SDS-PAGE (10%) (Bio-Rad Laboratories, Hercules, CA), transferred to nitrocellulose membranes, incubated using blocking buffer (LI-COR, Lincoln, NE), and immunoblotted with specific antibodies. The same antibodies used for METTL3 and BMAL1 immunohistochemical analysis were used for immunoblotting. The antibodies used for AHR (catalog number 83200) and CLOCK (catalog number 5157) are from Cell Signaling Technology, and CRY2 (catalog number 13997-1-AP), β-actin (catalog number 66009-1-Ig), laminB (catalog number 66095-1-Ig), and vinculin (catalog number 66305-1-Ig) are from Proteintech (Rosemont, IL). After incubation with appropriate secondary antibodies conjugated to infrared dyes (IRD-680 or IRD-800), the specific immune-reactive bands were visualized using the Odyssey CLx Imaging System (LI-COR) and quantified using ImageJ Studio software, version 5.2.

LC-MS Analysis of m^6A

RNA samples from four mice from each genotype were used for this study. Poly A RNA from 20 μg of total RNA was isolated by two rounds of purification through oligo-dT to minimize rRNA and tRNA contamination. Next, poly A^+ RNAs (approximately 35 ng per sample) were converted into individual nucleosides by successive digestions with nuclease P1 (2 hours at 42°C), followed by Fast Alkaline Phosphatase digestion (2 hours at 37°C). Mass spectrometry of nucleosides was performed using the Agilent 6460 Triple Quad MS-MS with 1290 ultrahigh-performance liquid chromatography. Five standards were used to calculate the concentration of each sample. A, G and m^6A concentrations were calculated based on standard curve, and means between technical replicate injections for each sample were calculated.

Quantitative Real-Time RT-PCR Analysis

Total RNA isolated from cells using TRIzol reagent (Thermo Fisher Scientific, Waltham, MA) was treated with DNase I and was converted into cDNA using high-capacity cDNA reverse transcription kit (catalog number 4351372; Thermo Fisher Scientific). Quantitative PCR was performed using 0.1 to 1 μg of cDNA with SYBR Green in a thermocycler. The fold difference in target gene mRNA levels was calculated using the ΔΔCT method and normalized to 18S rRNA or β-actin mRNA. The primer sequences are the following: Bmal1/Arntl, forward 5′-AGATGACGAACTGAAACACCTAA-3′, reverse 5′-GAAGACAGACTCGGAGACAAAG-3′, clock, forward 5′-GAGTGTTCAGTCCCTTGATGAG-3′, and reverse 5′-GCTGTGTCCCTATGACCATTT-3′. For Mettl3 quantitative real-time RT-PCR, TaqMan Fast Advanced Master Mix (catalog number 4444556), TaqMan assay for mouse Mettl3 (catalog number 4351372), and mouse glyceraldehyde-3-phosphate dehydrogenase (catalog number 4351372) kits (Thermo Fisher Scientific) were used following the manufacturer's instructions.

Isolation of Poly A^+ RNA

Whole livers from wild-type (WT) and M3LKO mice were immediately snap frozen and powdered on removal. To capture RNA, we resuspended powdered liver in TRIzol reagent (catalog number 15596018; Thermo Fisher Scientific). Total RNA was treated with DNase I (catalog number 04716728001, Roche Diagnostics, Indianapolis, IN) for 15

minutes at 37°C, cleaned with phenol/chloroform extraction, and resuspended in water. RNA concentration was measured using a NanoDrop. A total of 70 μg of DNase I–treated RNA was subjected to poly A^+ RNA enrichment per the manufacturer's protocol (catalog 61006; Thermo Fisher Scientific).

Fragmentation of Poly A^+ RNA

Poly A^+ RNAs were fragmented using a BioRuptor Pico sonication device to reach a mean fragment size of approximately 100 nucleotides. RNA fragments were ethanol precipitated, washed with 70% ethanol, and resuspended in water, and their concentration was measured using Qubit RNA HS Assay Kit (catalog number Q32855; Thermo Fisher Scientific).

meRIP Sequencing

A small amount of fragmented RNA (100 ng per sample) was aliquoted for use as input control. Another aliquot of fragmented RNA (1 μg of RNA per sample) was subjected to m^6A-enrichment using the EpiMark N6-Methyladenosine Enrichment Kit (catalog number E1610S, New England Biolabs, Ipswich, MA) per the manufacturer's protocol. First, 25 μL of protein G magnetic beads were used per sample and were washed and resuspended with 1× reaction buffer (150 mmol/L NaCl, 10 mmol/L Tris-HCl, pH 7.5, 0.1% NP-40). The washed beads were then incubated with 1 mL of N^6-methyladenosine antibody provided in the kit for 30 minutes at 4°C. Beads were washed and resuspended in 1× reaction buffer supplemented with 4 mL of RNase inhibitor (catalog number N8080119; Thermo Fisher Scientific). m^6A-IP fragmented RNA (1 mg per sample) was then incubated with α-m^6A-antibody–bound protein G beads for 1 hour at 4°C. Beads were then washed twice with the following buffers: 1× reaction buffer, 1× low salt reaction buffer (50 mmol/L NaCl, 10 mmol/L Tris-HCl, pH 7.5, 0.1% NP-40), and 1× high salt reaction buffer (500 mmol/L NaCl, 10 mmol/L Tris-HCl, pH 7.5, 0.1% NP-40). Beads were then resuspended in 30 mL of Buffer RLT (catalog number 79216; Qiagen, Germantown, MD). m^6A-immunoprecipitated RNA was cleaned and concentrated using EtOH precipitation, and concentrations were measured using the Qubit RNA HS Assay Kit (catalog number Q32855; Thermo Fisher Scientific).

Sequencing Library Preparation

The NGS Illumina Sequencing Library was prepared using Takara SMARTer Stranded Total RNA-Seq Kit v2 - Pico Input Mammalian (catalog number 634878; Takara Bio USA, San Jose, CA) per the manufacturer's protocol. Input and m^6A immunoprecipitation RNA from each sample was reverse transcribed using the next-generation sequencing kit (First Strand Synthesis Reaction, Illumina, San Diego, CA). Adaptors and indexes were then added to each sample individually and attached using PCR. The cDNA library was purified using AmPure XP PCR purification beads per manufacturer's protocol (catalog number A63882; Beckman-Coulter, Brea, CA). A second PCR was performed to amplify the final RNA sequencing libraries (15 cycles for m^6A immunoprecipitation RNA and 10 cycles for input RNA). Amplified libraries were cleaned and purified a second time with the AmPure XP PCR purification beads (catalog number A63882; Beckman-Coulter). Quality and concentration were checked using Bionalyzer High Sensitivity DNA Assay (catalog number 5067-4626; Agilent, Santa Clara, CA). Libraries were pooled to 3 nmol/L and run on Illumina Hi-Seq with the following settings: single-read 50 bp and pooled on two lanes.

m^6A MeRIP Sequencing Data Analysis

MeRIP sequencing reads were aligned to mouse genome mm10 with HISAT2 version 2.1.0 (*https://github.com/DaehwanKimLab/hisat2*),[35] with splice site reference annotation ENSEMBL version 96 (*ensembl.org*). Only uniquely mapped and nonduplicated reads were selected by samtools version 1.4 (*http://www.htslib.org*).[36] The generated BAM files were then used for m^6A peak calling using exomePeak software version 3.8 (*https://bioconductor.riken.jp/packages/3.8/bioc/html/exomePeak.html*).[36] ExomePeak was also used for differential m^6A level analysis between WT and M3LKO mice using a fragment length of 50 nucleotides. Peak sites were assigned and annotated to 5′-UTR, coding sequence, 3′-UTR, and transcription start site, using transcript information for mouse ENSEMBL version 96. The raw meRIP sequencing data (BAM files) were submitted to the GEO database (*www.ncbi.nlm.nih.gov/geo*; accession number GSE179680).

RNA Sequencing Data Analysis

Libraries from the input RNA were used for RNA sequencing analysis. Analysis of RNA sequencing was performed with a combination of kallisto[37] and sleuth.[38] Transcript annotation indexes for mouse kallisto were created from FASTA files from the mouse ENSEMBL release 96 with a k-mer length of 19 (-k 19). Kallisto quantification was performed on single-end RNA sequencing (-single -l 50 -s 1) data with the respective transcript index and 100 bootstraps (-b 100). The kallisto output was next analyzed with sleuth for differential expression at gene-level annotation. Gene names and attributes were queried from ENSEMBL using biomaRt. The raw RNA sequencing data were submitted to the GEO database (*www.ncbi.nlm.nih.gov/geo*; accession number GSE176113).

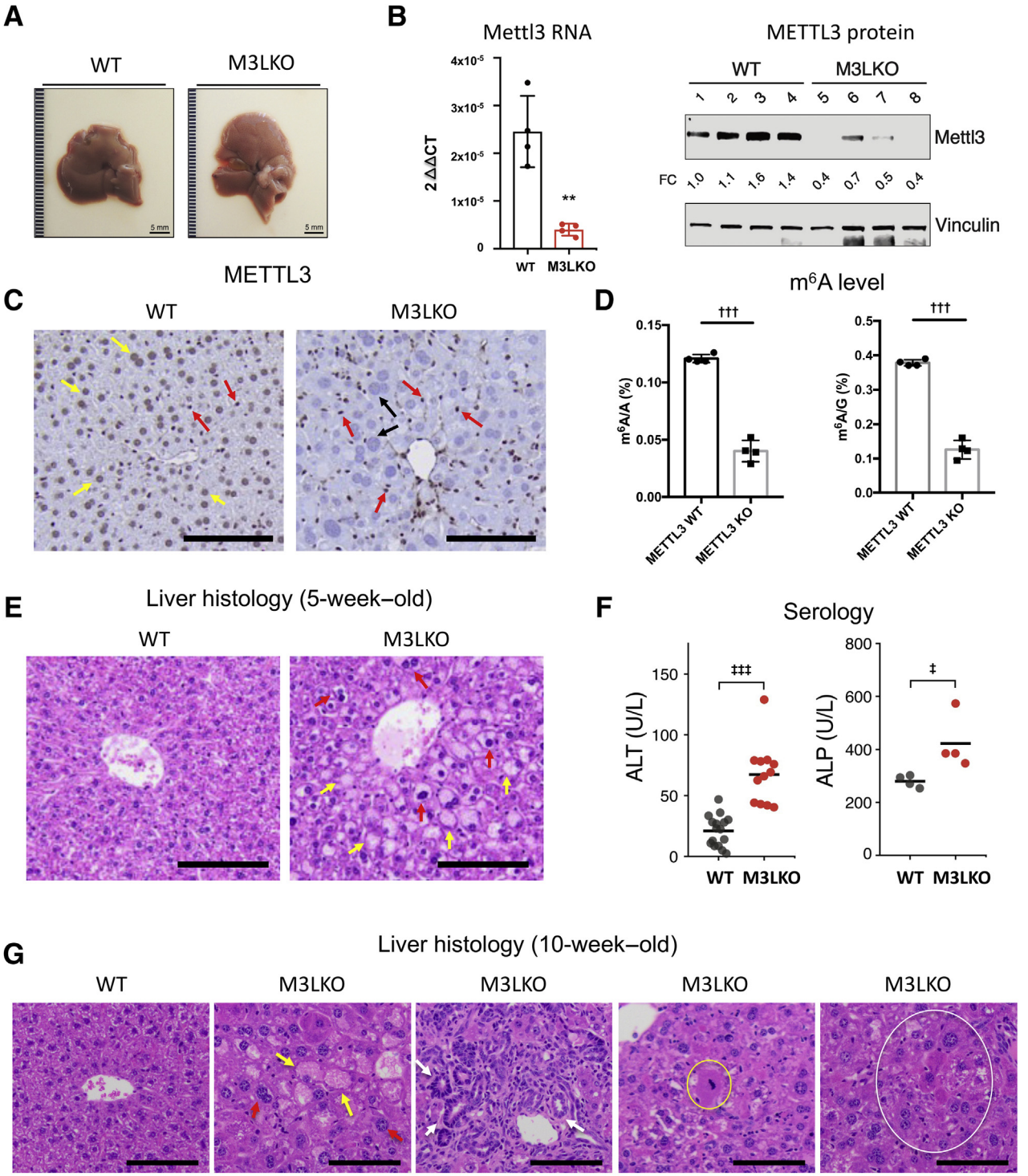

Figure 1 Histopathologic analysis of young adult liver-specific METTL3 knockout (M3LKO) mice demonstrates development of abnormal liver architecture and function. **A:** Representative liver pictures of 5-week—old wild-type (WT) and M3LKO mice. **B:** METTL3 depletion in M3LKO mice demonstrated by quantitative real-time RT-PCR (**left panel**) and immunoblotting of whole liver extracts (**right panel**). **C:** Immunohistochemical analysis demonstrates METTL3 depletion in the hepatocytes but not in nonparenchymal cells (NPCs). **Yellow**, **red**, and **black arrows** denote WT hepatocytes, NPCs, and M3LKO hepatocytes, respectively. **D:** Liquid chromatography—mass spectrometryanalysis of m^6A residues in liver poly A^+ RNA represented as m^6A/A and m^6A/G showed significant decrease in the WT and M3LKO mice. **E:** Representative microscopic pictures of formalin-fixed, paraffin-embedded liver sections of 5-week—old mice stained with hematoxylin and eosin (H&#). **Yellow** and **red arrows** denote ballooned (steatotic/apoptotic) and pleomorphic hepatocytes, respectively. **F:** Analysis of serum alanine phosphatase (ALP) and alanine aminotransferase (ALT) in 5-week—old mice. **G:** Representative images of H&E-stained liver sections of 10-week—old mice demonstrated apoptotic hepatocytes (**yellow arrows**), pleomorphic nuclei (**red arrows**), ductular reactions (**white arrows**), mitotic (**yellow circle**), and foci of altered hepatocytes (**white circle**). Data are expressed as relative METTL3 expression per sample (**B**). $^{**}P < 0.01$ versus WT; $^{†††}P < 0.001$ (*t*-test); $^{‡}P < 0.05$, and $^{‡‡‡}P < 0.001$ (Welch *t*-test). Scale bars = 5 mm (**A**); 200 μm (**C** and **E**); 100 μm (**G**).

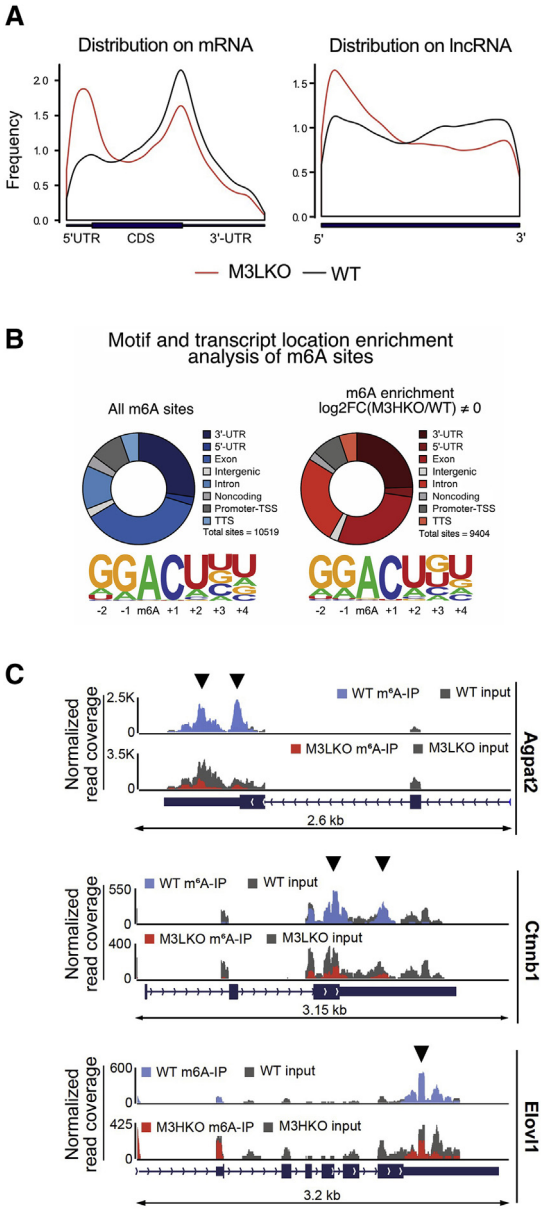

Figure 2 Methylated (m^6A) RNA immunoprecipitation (meRIP) coupled with sequencing analysis identifies polyadenylated RNAs with reduced m^6A methylation at their 3′-UTRs and exons in liver-specific METTL3 knockout (M3LKO) livers compared with WT livers. **A:** Normalized distribution of high-confidence m^6A sites on mRNAs and long noncoding RNAs (lncRNAs) in 5-week–old wild-type (WT) and M3LKO mice. Black lines indicate distribution of all m^6A sites identified. Red lines denote distribution of all m^6A sites found to have significantly altered enrichment in M3LKO livers (fold change in m^6A enrichment (WT/M3LKO $\neq$ 0). Significant enrichment was calculated using ExomePeak finder with a rescaled hypergeometric test false discovery rate cut-off of $P < 0.05$ and absolute fold change enrichment >1. **B:** Motif enrichment for each peak type (all sites or altered sites) was identified by running Homer Motif Analysis. Only the most significant and prevalent motifs are shown. **C:** Peak distribution normalized to input in the genomic regions of 3 critical transcripts (*Agpat2*, *Ctnnb1*, and *Elovl1*) in the WT and M3LKO mice are shown. Sequencing tracks of these genes and enrichment in the m^6A immunoprecipitation and input in the WT and M3LKO livers were visualized using Integrated Genome Viewer (IGV) software version 2.4.16 (Broad Institute, Cambridge, MA). **Arrowheads** indicate m^6A peaks. $n = 4$ per genotype (**A**). TSS, transcription start site; TTS, transcription termination site.

Fluorescence Microscopy of Liver Sections and Counting of Binucleate Hepatocytes

Livers from 2-, 5- and 10-week–old M3LKO and WT mice were stained for β-catenin to mark cell membranes and Hoechst dye to mark nuclei as previously described.[39] Briefly, after paraffin embedding, sectioning, and antigen retrieval, liver sections were blocked with 2% bovine serum albumin. For quantification of mononucleate and binucleate hepatocytes, sections were stained with mouse anti–β-catenin primary antibody (catalog number sc-7199; Santa Cruz, Dallas, TX) followed by goat anti-mouse AlexaFluor 594 secondary antibody (catalog number A11055; Invitrogen, Carlsbad, CA). The sections were counterstained with Hoechst 33342 (Invitrogen) and mounted with Fluoromount-G (Southern Biotech, Birmingham, AL). A minimum of 700 hepatocytes per sample were scored.

Ploidy Analysis

Nuclei were isolated from whole liver tissue as previously described.[40] Briefly, livers were mashed through a 100-μm pore size strainer. Cell suspension was resuspended in 0.25 mol/L sucrose buffer [0.25 mol/L sucrose, 5 mmol/L $MgCl_2$, and 10 mmol/L Tris-HCl (pH 7.4)] and was centrifuged at 600 × *g* for 10 minutes at 4°C. The supernatant was kept as the cytoplasmic fraction, and the pellet was washed with 0.25 mol/L sucrose buffer. The crude nuclear pellet was resuspended in 2 mol/L sucrose buffer [2 mol/L sucrose, 10 mmol/L Tris-HCl (pH 7.4), and 1 mmol/L $MgCl_2$] and mixed well. The nuclei suspension was centrifuged at 16,000 × *g* at 4°C for 30 minutes. The bottom white pellet was kept as nuclei, and the brown fraction was discarded. Nuclei were then subjected to flow cytometry after staining with propidium iodide.

Statistical Analysis

Statistical analysis was performed using GraphPad Prism software version 9.1.2 (GraphPad Software, San Diego, CA) or R software version 3.5.2 (R Foundation for Statistical Computing, Vienna, Austria). A Wald test, Welch test, *U*-test, or *t*-test was used in most cases, depending on the types of variables in the data collected.

Results

Deletion of Mettl3 in Neonatal Mouse Livers Results in Nuclear Pleomorphism, Hepatocyte Ballooning, and Ductular Reaction

To uncover the consequences of m^6A depletion from polyadenylated RNAs in the liver, M3LKO mice were generated by crossing *Mettl3*$^{fl/fl}$[15] mice with *Alb-Cre* mice.[30] Genotypes of mice were confirmed by tail DNA PCR (Supplemental Figure S1A). The body and liver weights of 5-week–old

M3LKO mice were comparable to those of the control WT mice (*Mettl3*$^{+/+}$; *Alb-Cre*, or *Mettl3*$^{fl/fl}$) (Supplemental Figure S1B). Macroscopically, M3LKO livers appeared normal, although they were slightly pale (Figure 1A). The *Mettl3* RNA level was reduced by approximately 70%, and the protein level decreased by 50% to 60% in whole livers from homozygous M3LKO mice (Figure 1B). METTL3 localized in hepatocyte nuclei in control WT mice (Figure 1C), as indicated by immunohistology. In contrast, METTL3 was detectable predominantly in nonparenchymal cells in M3LKO livers, whereas hepatocyte nuclei were bigger and essentially devoid of METTL3 (Figure 1C). Functional depletion of METTL3 was confirmed by quantifying methylated adenosine residues in liver poly A$^+$ RNAs by mass spectrometry. The significant decrease in m^{6}A/A and m^{6}A/G ratios indicates that METTL3 is critical for adding m^{6}A marks in polyadenylated RNAs (Figure 1D).

Examination of the H&E-stained liver sections revealed hepatocytes with pleomorphic nuclei (nuclei of different sizes and shapes), microsteatosis (small lipid droplet accumulation), and hepatocyte ballooning (degeneration) in 5-week−old M3LKO mice compared with WT controls (Figure 1E). Increased microsteatosis in M3LKO livers was confirmed by accumulation of lipids in the liver by Oil-Red-O staining (Supplemental Figure S1C). A small but significant increase in serum alanine aminotransferase levels and significantly higher serum alkaline phosphatase levels (Figure 1F) indicated modest liver injury in M3LKO mice. Histopathologic analysis of 10-week−old M3LKO mice demonstrated similar phenotype as observed in 5-week−old mice; however, the number of enlarged hepatocytes with bigger nuclei and cholangiocyte hyperplasia was more pronounced (Figure 1G). Scattered apoptotic (Supplemental Figure S1D), mitotic, and foci of altered hepatocytes (Figure 1G), indicative of preneoplastic changes,[41] were also detected in M3LKO mice. Collectively, these results indicate that lifelong METTL3 depletion caused liver injury and deranged liver microscopic structure in mice.

Widespread Changes in the m^{6}A Methylome and Expression Profile of the Liver Transcriptome in M3LKO Mice

Because depletion of METTL3 reduced global m^{6}A level in the liver (Figure 1D), the next step was to determine how the hepatic m^{6}A landscape in mRNA was altered by METTL3 depletion using meRIP sequencing analysis. Poly A$^+$ RNAs from the M3LKO and WT control livers were immunoprecipitated with an m^{6}A-specific antibody, and cDNA libraries generated from both the input and pull-down RNAs were sequenced. Sequences enriched in the immunoprecipitated RNAs relative to input RNAs are considered as transcripts that contain m^{6}A methylation. Genomic annotation of meRIP sequencing data indicated that most m^{6}A sites were in 3′-UTRs, although m^{6}As were identified throughout the length of hepatic mRNAs in both genotypes (Figure 2A). Among these sites, the overall enrichment of m^{6}A was reduced in 3′-UTRs and exons but increased in 5′-UTRs of mRNAs in M3LKO livers. Similarly, loss of m^{6}A at the 3′-ends of long noncoding RNAs (lncRNAs) was also noted in M3LKO livers (Figure 2A).

A total of 10,850 and 754 regions of high-confidence m^{6}A sequences (m^{6}A peaks) were identified by meRIP sequencing in mRNAs and lncRNAs, respectively (Table 1). Among these, 4965 m^{6}A peaks were lost and 3121 were gained in mRNAs in M3LKO livers, whereas 384 m^{6}A peaks were lost and 196 gained m^{6}A in lncRNAs in M3LKO livers. The increase in m^{6}A peaks in 3′-UTRs and exons and especially the greater than two-fold increase in 5′-UTRs of certain transcripts (Table 1) could be attributable to enrichment/recruitment of progenitor/oval cells and nonparenchymal cells (eg, hematopoietic cells, inflammatory cells, and endothelial cells) that express METTL3. Increased expression or activity of another uncharacterized m^{6}A methylase in hepatocytes might also contribute to increase in certain m^{6}A peaks. The two most prevalent motifs, namely [GGm^{6}AC(U>A)(U>G>C>A)(U>A>G>C)] and [GGm^{6}AC(U>A)(G>U>C>A)(U>G>A>C)], were found not only in the 5′- and 3′-UTRs but also in exons, introns, transcription start, and termination sites of mRNAs, lncRNAs, and intergenic transcripts (Figure 2B). For example, there was marked decrease in enrichment of m^{6}A RNA relative to input RNA in the 3′-UTRs of metabolic transcripts *Agpat2*, *Ctnnb1*, and *Elovl1* (Figure 2C) in the M3LKO mouse livers when compared with WT mouse livers.

Next, the impact of the global changes in hepatic m^{6}A levels observed in M3LKO mice on the liver transcriptome was assessed by sequencing poly A$^+$ RNAs from the meRIP sequencing analysis described in Figure 2A. A cumulative fraction plot of the RNA sequencing data revealed that transcripts with reduced m^{6}A enrichment in M3LKO livers [$\log_2$ fold change (FC)(WT/M3LKO) $>$ 0] resulted in increased transcript steady-state levels. However, in general, transcripts with increased or no unchanged m^{6}A levels in M3LKO livers relative to the control livers

Table 1 Total Number of m^{6}A Peaks in the Murine Liver and Their Alterations in M3LKO Mice

	mRNA				
m^{6}A peaks in M3LKO mice	5′-UTR	Exon	3′-UTR	Total	lncRNA
Reduced	253	2251	2461	4965	384
Increased	589	1405	1127	3121	196
No change	233	1323	1208	2764	174
Total	1075	4979	4796	10,850	754

The total number of peaks (transcript sequences) that were identified in the wild-type liver that exhibited m^{6}A enrichment in immunoprecipitated RNA with the m^{6}A-specific antibody compared with input RNA are given. Enrichment of these sites were then compared in M3LKO versus WT mice to identify differential peaks.

lncRNA, long noncoding RNA; M3LKO, liver-specific *Mettl3* knockout.

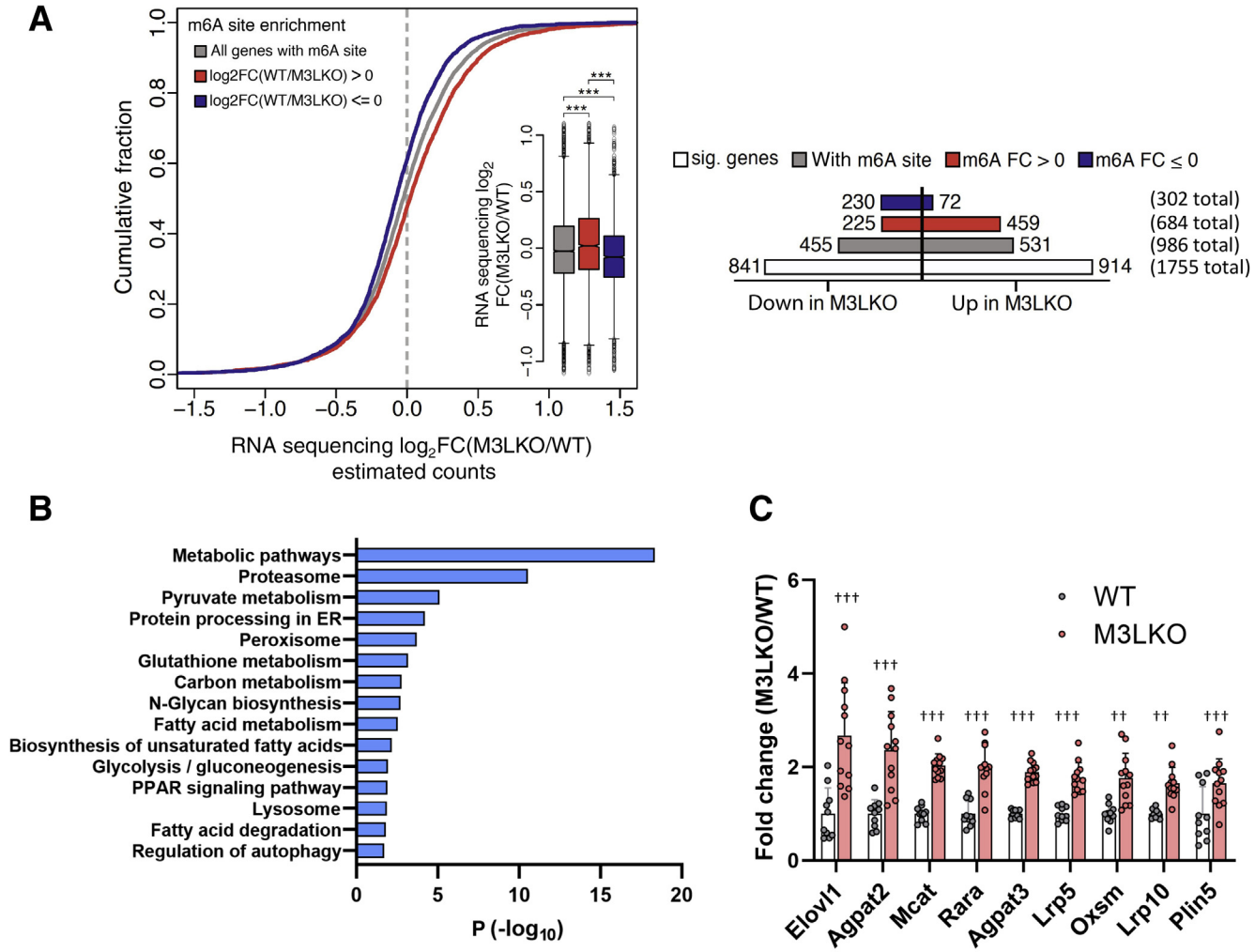

Figure 3 RNA sequencing (RNA-seq) analysis reveals polyadenylated RNAs are differentially expressed in liver-specific METTL3 knockout (M3LKO) livers compared with wild-type (WT) mice livers. **A:** Cumulative fraction plot of poly A^+ RNA expression in response to m^6A enrichment (**left panel**). Transcripts were grouped in the following ways: those harboring m^6A sites (gray), those with sites exhibiting reduced or lost m^6A methylation [red; m^6A enrichment $\log_2$ fold change (FC)(WT/M3LKO) > 0], and those with m^6A sites with increased or unchanged methylation [blue; m^6A enrichment $\log_2$FC(WT/M3LKO) ≤ 0] in M3LKO livers relative to the WT livers. **Inset:** Box plots depict differential poly A^+ RNA abundance in these three groups classified based on m^6A site enrichment. A horizontal bar plot (**right panel**) depicting the overall number of significantly altered transcripts (Welch test) in the following groups, from top to bottom, is presented: transcripts enriched or unaltered in M3LKO ($m^6A \leq 0$) (302 total; blue bar), transcripts harboring m^6A sites lost in M3LKO livers ($m^6A > 0$) (684 total; red bar), transcripts with m^6A marks in both (986 total; gray bar), and all transcripts (with and without m^6A) (1175 total; unfilled bar). **B:** The Kyoto Encyclopedia Gene and Genome pathway analysis of genes significantly dysregulated in M3LKO livers relative to WT livers in 5-week–old mice. **C:** RNA sequencing data demonstrating significant up-regulation of expression of select genes with m^6A marks involved in metabolic pathways in M3LKO livers compared with WT livers (M3LKO/WT). $n = 6$ for WT (4 male and 2 female) mice; $n = 8$ M3LKO (4 male and 4 female) mice. $^{***}P < 0.001$ (*U*-test); $^{\dagger\dagger}P < 0.01$, $^{\dagger\dagger\dagger}P < 0.001$ (Wald *t*-test). ER, estrogen receptor; PPAR, peroxisome proliferator-activated receptor; sig., significant.

[$\log_2$FC(WT/M3LKO) $\leq$ 0] were down-regulated or unchanged in the mutant livers (Figure 3A). A Welch *t*-test identified deregulation of 1755 transcripts ($P < 0.001$) in the mutant livers (Figure 3A). Among these transcripts, 986 (56%) were detected with m^6A in the WT and/or mutant livers, suggesting indirect regulation of the remaining 44% of transcripts. Among 684 transcripts with loss of m^6A in M3LKO livers, 459 were up-regulated and 225 were down-regulated. Among 302 transcripts with increased or unchanged m^6A levels in M3LKO livers, 230 were suppressed and 72 were induced.

The Kyoto Encyclopedia Gene and Genome pathway analysis of the RNA sequencing data revealed a significant dysregulation of metabolic pathways (eg, pyruvate, glutathione, fatty acid, glycolysis, and gluconeogenesis) as well as proteosome and peroxisome proliferator-activated receptor signaling in M3LKO livers (Figure 3B). Intriguingly, alterations in lipid metabolic pathways correlated with increased microsteatosis in M3LKO mice (Supplemental Figure S1C). Moreover, m^6A marked metabolic transcripts (eg, *Elovl1*, *Lrp5*, *Lrp10*, *Mcat*, *Oxsm*, and *Rarα*), including *Agpat2* and *Agpat3,* which encode enzymes involved in

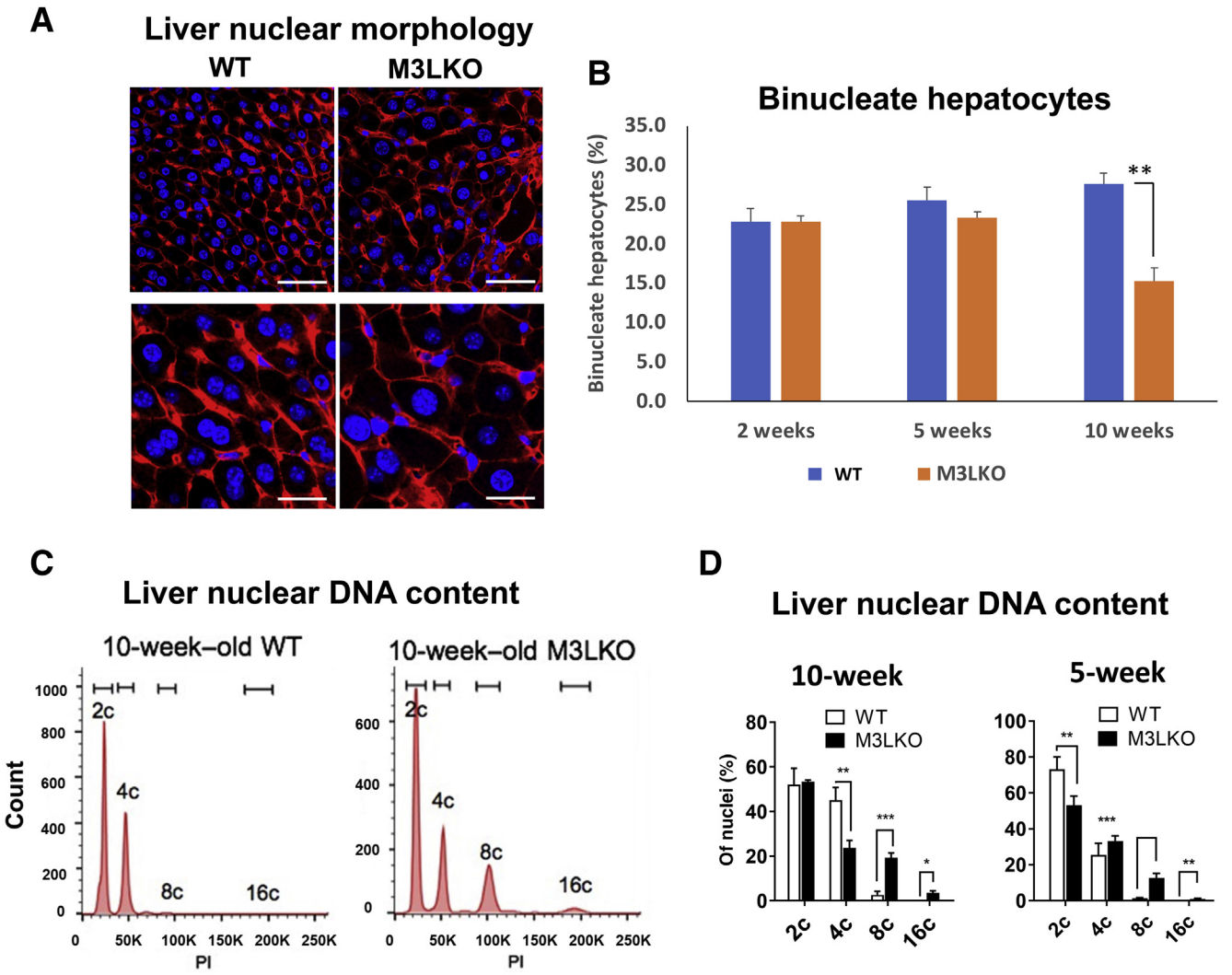

Figure 4 METTL3-depleted hepatocytes exhibit reduced binuclearity and increased polyploidy. **A:** Fluorescence microscopic pictures of liver sections from wild-type (WT) and liver-specific METTL3 knockout (M3LKO) mice stained with β-catenin antibody for membrane (red) and Hoechst dye for nuclei (blue), respectively. Representative images of 10-week–old mouse livers are shown. **B:** Binucleate hepatocytes of 2-, 5-, and 10-week–old mice were counted in several fields and the relative populations in WT and M3LKO (3 mice per genotype per age group) mice are presented. **C** and **D:** DNA content of freshly isolated liver nuclei was determined by flow cytometry after staining with propidium iodide (PI). The percentage of nuclei with 2c, 4c, 8c, and 16c DNA content was determined using FlowJo software version 9.9.6 (Beckton Dickinson, Ashland, OR). Representative ploidy profiles are shown for 10-week–old WT and M3LKO mice (**C**), and the percentage of each ploidy population is summarized at 5 and 10 weeks (**D**). $n = 3$ mice per genotype. $^{*}P < 0.05$, $^{**}P < 0.01$, and $^{***}P < 0.001$ (*t*-test). Scale bars: 50 μm (**A**, **top row**); 25 μm (**A**, **bottom row**).

triglyceride synthesis, were significantly up-regulated in M3LKO livers (Figure 3C). In WT livers, meRIP sequencing identified one or more m^6A peaks in each transcript, and at least one peak was reduced in the mutant mice (Supplemental Table S1).

Pleomorphism in M3LKO Hepatocytes Correlates with Decreased Binucleation and Increased Nuclear Polyploidy

Next, hepatic nuclear pleomorphism in M3LKO mice was investigated (Figure 1, E and G), an observation that was confirmed by fluorescence microscopy of Hoechst- and β-catenin–stained liver sections to visualize nuclei and cell membranes, respectively (Figure 4A). The sizes of the hepatocytes and nuclei were larger in M3LKO mice compared with those of age-matched controls. Hepatocytes are characterized by variations in polyploidy defined as an increase in the number of chromosome sets and is regulated by the number of nuclei per cell (typically one or two) and DNA content of each nucleus.[42] Notably, the binucleate hepatocyte population was reduced by approximately 50% in M3LKO mice at 10 weeks of age (Figure 4B), indicating altered hepatocyte ploidy. To determine whether nuclear ploidy contributes to the pleomorphic nuclei in M3LKO livers, the DNA content of propidium iodide–stained nuclei was measured by flow cytometry. The results indicated that the M3LKO

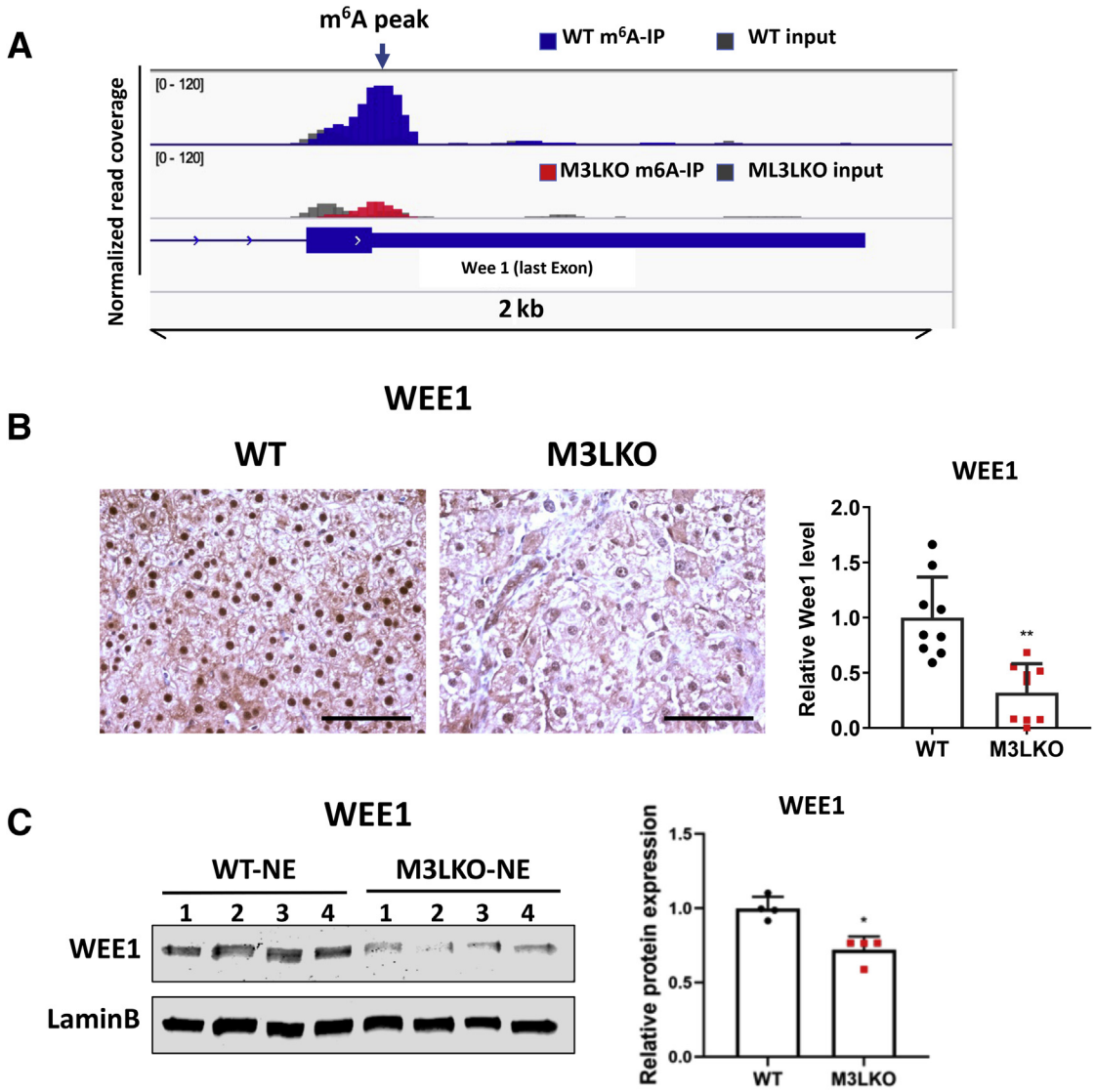

Figure 5 WEE1 protein is down-regulated in liver-specific METTL3 knockout (M3LKO) livers. **A:** Methylated (m^6A) RNA immunoprecipitation coupled with sequencing identified an m^6A peak (denoted by an **arrow**) in the last exon of *Wee1* transcript in the wild-type (WT) livers, which was reduced in M3LKO livers of 5-week–old mice. **B** and **C:** Immunohistochemical and immunoblot analyses showed significant decrease in WEE1 protein in 10-week–old mice. WEE1-positive nuclei were counted in three randomly selected field in each liver section. $n = 4$ per genotype. $^*P < 0.01$, $^{**}P < 0.001$ versus WT. Scale bars = 50 μm.

mice had more hepatocyte nuclei with 8c and 16c DNA content compared with those of the WT mice at 5 and 10 weeks of age (Figure 4, C and D). Increased nuclear ploidy was noted predominantly in male mice (female data not shown).

In addition to ploidy change, hepatocytes from 10-week–old M3LKO mice were also highly proliferative and showed signs of DNA damage as revealed by Ki-67 and phospho-γ-H2a.x immunohistochemical analysis, respectively (Supplemental Figure S1, E and F). Consistent with this, RNA sequencing data revealed significantly up-regulated expression of genes involved in cell cycle control (eg, *Bcl9l*, *Ccnb1*, *Ccnb2*, *Cdk1*, *Cdk9*, *Chk1*, *E2f1*, *Mcm6*, and *Rpa1*) and P53 target genes associated with DNA damage and repair response and apoptosis in M3LKO livers (eg, *Aen*, *Bax*, *Bbc3*, *Btg2*, *Cdkn1a*, *Fas*, *Gdf15*, *Ploh*, and *Tigar*) (Supplemental Figure S1, G and H). Among these transcripts, *Aen*, *Bax*, *Bbc3*, *Bcl9l*, *Btg2*, *Cdk9*, *Gdf15*, *Mcm10*, *Rpa1*, and *Tigar* had one or multiple m^6A peaks in the WT livers, at least one of which was reduced in M3LKO livers (except for *Bax*) (Supplemental Table S1). Among 237 genes reported to encode proteins involved in polyploidy,[43] 36 genes were significantly dysregulated in M3LKO livers (eg, *Arf6*, *Bcl2l1*, *Becn1*, *Cdkn1a*, *E2f1*, *E2f3*, *E2f4*, *Limk1*, *Limk2*, *Nedd4l*, *Plk3*, and *Src*) (Supplemental Table S2). Among these, only *Arf6*, *Bcl2l1*, and *Limk2* with m^6A mark in WT livers were reduced in M3LKO (Supplemental Table S1), suggesting indirect regulation of the other transcripts. These results suggest that the depletion of METTL3 causes hepatocyte death, which may lead to compensatory proliferation of surviving hepatocytes. Ploidy regulation is disrupted, resulting in delayed

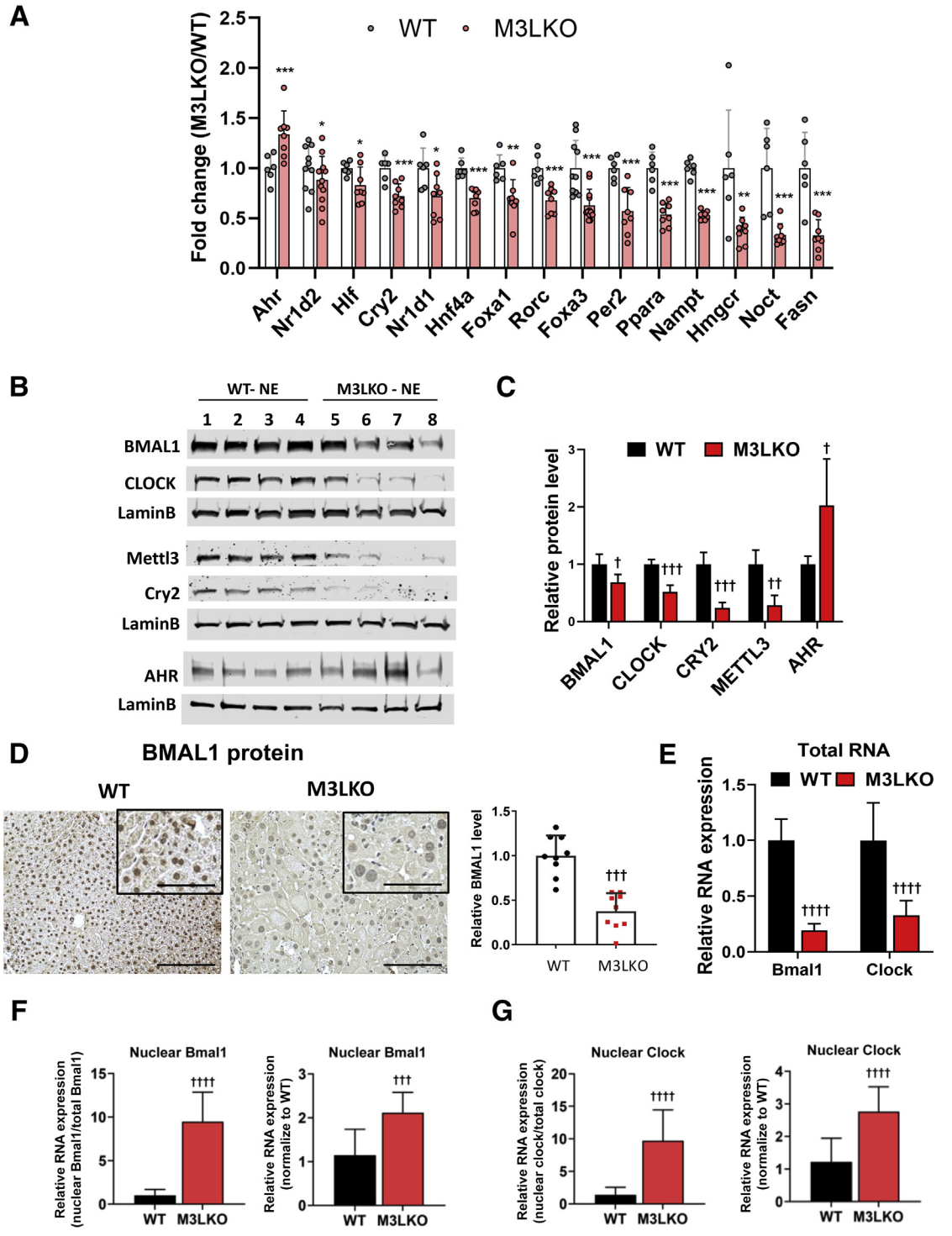

Figure 6 BMAL1 and CLOCK protein levels are significantly reduced in the livers of 10-week—old liver-specific METTL3 knockout (M3LKO) mice compared with wild-type (WT) mice. **A:** RNA sequencing data demonstrating dysregulation of circadian rhythm—controlled genes in livers of 5-week—old M3LKO mice. **B:** Immunoblotting of selected proteins involved in circadian rhythm control in liver nuclear extracts (NEs) of 10-week—old WT and M3LKO female mice. **C:** The mean values in the WT mice were assigned as 1. The data were quantified using Image Studio software version 5.2 (LI-COR, Lincoln, NE). **D:** Representative pictures of BMAL1 immunohistochemical analysis in WT and M3LKO liver sections of 10-week—old mice are shown. Quantification of BMAL1 level using ImageJ software version 1.52a (NIH, Bethesda, MD; *http://imagej.nih.gov/ij*) was performed by counting positive cells in three randomly selected fields. **E:** Quantitative real-time RT-PCR analysis of *Bmal1* and *Clock* mRNAs from whole liver of 10-week—old WT and M3LKO mice. **F** and **G:** *Bmal1* and *Clock* mRNAs in the liver nuclear fraction of mice. *Mettl3* mRNA expression was normalized to the respective levels in the M3LKO liver or in the WT liver using the same amount of cDNA of each fraction or total liver. Data are expressed as means ± SD (**A, C, E**—**G**). $n = 3$ (**D**); $n = 4$ per genotype per sex (**C**, **F**, and **G**). $^{*}P < 0.05$, $^{**}P < 0.01$, $^{***}P < 0.001$ versus WT (Wald *t*-test); $^{\dagger}P < 0.05$, $^{\dagger\dagger}P < 0.01$, $^{\dagger\dagger\dagger}P < 0.001$ and $^{\dagger\dagger\dagger\dagger}P < 0.0001$ versus WT (*t*-test). Scale bars: 100 μm (**D**); 50 μm (**D, insets**).

or compromised cytokinesis and enrichment of mononucleate hepatocytes with highly polyploid nuclei.

Next, expression of the cell cycle kinase-encoding gene, *Wee1*, identified as an m^{6}A marked transcript in ESCs[14] and HeLa cells,[44] was determined. WEE1 negatively regulates cell cycle (G2-M) progression by inactivating cyclin B−Cdk1 kinase via phosphorylating Cdk1. Indeed, meRIP sequencing data identified an m^{6}A peak in *Wee1's* last exon near the stop codon in the WT but not in M3LKO livers (Figure 5A).[44] Immunohistochemical analyais and immunoblotting data indicated a significant decrease in WEE1 protein level in M3LKO hepatocytes nuclei and liver nuclear extracts, respectively (Figure 5, B and C). These results suggest down-regulation of WEE1 may perturb hepatic cell cycle progression in M3LKO mice.

Genes Involved in Circadian Rhythm Control Are Deregulated in M3LKO Livers

Molecular clocks, such as BMAL1/ARNTL, CRY, and PER in peripheral tissues, are involved in coordinating cellular processes, such as metabolism, cell cycle, and DNA repair.[45] Inhibition of m^{6}A modification by addition of 3-deazaadenosine, a transmethylation inhibitor or depletion of METTL3, lengthens and dampens the circadian period in U2OS and mouse embryonic fibroblast cells by delaying RNA processing.[46] Circadian-gated rhythms of hepatocyte polyploidy have also been reported in rodents.[47] Hence, it was of interest to know whether core clock genes or clock-regulated genes are deregulated in M3LKO livers, which could contribute to the metabolic and ploidy change in the mutant mice. Comparison of the RNA sequencing data revealed that expression of circadian rhythm−controlled transcripts (eg, *Ahr*, *Cry2*, *Foxa1*, *Foxa3*, *Fasn*, *Hlf*, *Hmgcr*, *Hnf4α*, *Nampt*, *Noct*, *Nr1d1*, *Nr1d2*, *Per2*, *Pparα*, and *Rorc*) were altered in livers of M3LKO mice compared with the WT controls (Figure 6A). Among these transcripts, all except *Nampt* harbored m^{6}A peaks in the WT livers, and at least one m^{6}A peak was reduced in M3LKO livers (Supplemental Table S1). Almost all these genes, with the exception of *Ahr*, were down-regulated in M3LKO livers. To uncover the mechanism for down-regulation of circadian rhythm−controlled genes in M3LKO livers, the levels of core clock transcription factors BMAL1/ARNTL and CLOCK were assessed. Immunoblot analysis found a marked reduction in nuclear BMAL1, CLOCK, and their target CRY2 protein levels in both male and female M3LKO mice that correlated with the decrease in METTL3 level (Figure 6, B and C). Only the AHR level was increased in the mutant livers, suggesting its up-regulation probably occurred independently of BMAL1-CLOCK. Immunohistochemical analysis confirmed a reduced BMAL1 level in M3LKO hepatocytes (Figure 6D). Interestingly, quantitative real-time RT-PCR data revealed that steady-state *Bmal1/Arntl* and *Clock* mRNAs were reduced in M3LKO livers (Figure 6E) but increased in the nuclear fraction when normalized to total RNA or their respective levels in the WT livers (Figure 6, F and G), suggesting nucleocytoplasmic export of their mRNAs might be impeded in mutant livers. Collectively, these data suggest that significant decreases in the nuclear levels of BMAL1 and CLOCK could be one of the mechanisms involved in the suppression of clock-controlled genes in METTL3-depleted livers, many of which regulate metabolism.

Discussion

In the present study, the physiologic function of METTL3 was investigated in the liver using mice with *Mettl3* deleted at the neonatal stage. M3LKO mice were born in expected mendelian ratios, and they did not exhibit early mortality compared with WT mice. Multiple assays indicated that *Mettl3* loss disrupted hepatocyte architecture and differentiation/maturation state. M3LKO livers exhibited larger hepatocytes with bigger and irregular nuclear size and reduced binucleate hepatocyte population. The proliferative hepatocytes and bile duct cells (cholangiocytes) suggested impaired hepatocyte differentiation and maturation. Importantly, loss of METTL3 in hepatocytes caused increased nuclear polyploidy, microsteatosis, and dysregulated expression of genes involved in metabolism, cell cycle control, and regulation of circadian rhythms.

Role of METTL3 in the Maintenance of Hepatic Differentiation State and Liver Cancer

A complex network of liver-enriched transcription factors (LETFs) (eg, *C/ebpα*, *Foxa1-a3 (HNF3 α,β,γ)*, *HNF4α*, *Onecut1/2* and *Hnf6α,β*) are critical in the maintenance of the differentiation state of hepatocytes.[48,49] Concerted action of these factors is essential for liver development. *Mettl3* depletion impairs mouse and human ESCs to differentiate into different lineages but promotes their self-renewal ability both *in vitro* and *in vivo*.[14,15] Marked down-regulation of LETFs and their downstream targets and up-regulation of *Gata6*, a fetal transcription factor, and *Sox9*, a cholangiocyte-specific transcription factor, suggest a progenitor cell phenotype of *Mettl3*-depleted hepatocytes. These results suggest that METTL3 is essential for the maintenance of a postnatal hepatocyte differentiation state in mice.

There are contradictory reports on the role of m^{6}A and METTL3 on hepatocarcinogenesis. One study reported that the m^{6}A level in mRNA was reduced in primary human hepatocellular carcinoma (HCCs) compared with the benign livers, which correlated with down-regulation of METTL14, the RNA binding partner of METTL3.[13] Another study reported that *METTL3* RNA level was up-regulated in human HCCs compared with benign livers, which correlated with poor prognosis.[50] METTL3 overexpression promotes growth of HCC cell lines *in vitro* and *ex vivo* by increasing m^{6}A marks in the *SOCS2* transcript. However, this study

neither showed METTL3 protein levels in human primary HCCs nor explored the consequence of METTL3 depletion in normal hepatocytes. The consequence of METTL3 depletion in hepatocytes, which may induce their dedifferentiation and proliferation as observed in M3LKO ESCs,[14] has not been reported. Hyperplasia of hepatocytes, cholangiocytes, and oval cells[51] and appearance of mitotic and foci of altered hepatocytes presented as preneoplastic lesions in animal models of hepatocarcinogenesis[41] in M3LKO mice as early as 5 to 6 weeks of age, suggesting that these mice might develop spontaneous HCC and/or cholangiocarcinoma with age or after treatment with liver carcinogens.

Role of METTL3 in Regulating Liver Circadian Rhythm

The connection between m^{6}A and circadian rhythm has been demonstrated by the inhibition of m^{6}A methylation by deaza-adenosine or siRNA-mediated METTL3 depletion that delayed mRNA export to the cytoplasm and extended the circadian clock in U2OS and mouse embryonic fibroblast cells; in contrast, overexpression of catalytically active METTL3 increased clock oscillator speed.[46] The RNA sequencing data in 5-week−old mice revealed that expression of key components of the molecular clock timing mechanism [*Cry1/2*, *Per1/2*, *Nfil3*, *Rev-Erbα,β (Nr1d1/2)*, and *ROR-α,β,γ*] and many of their downstream targets (*Dbp*, *Fasn*, *Hlf*, *Hmgcr*, *Noct*, *Nampt*, *Pparα*, *Mtnr1a*, and *Tef*) are deregulated in M3LKO livers. Furthermore, both BMAL1 and CLOCK, two master transcription factors that cooperatively regulate many clock-control genes, are significantly reduced in M3LKO livers compared with WT livers. Collectively, these results indicate that the liver circadian rhythm is perturbed in M3LKO mice. It could be postulated that the hepatic clock is disrupted in M3LKO mice. Expression of BMAL1 and CLOCK are regulated at multiple levels, including by transcriptional, post-transcriptional, and posttranslational mechanisms (eg, phosphorylation and ubiquitination).[52−55] Rhythmic nuclear entry of BMAL1 also regulates clock timing.[56] Because accumulation of *Bmal1* and *Clock* mRNA in the nuclei of M3LKO mice was noted, it is tempting to speculate that decreased synthesis of BMAL1 and CLOCK proteins is likely attributable to inhibition of mRNA export, although further regulation at the level of translation, posttranslational modifications, and/or nuclear import of these proteins in M3LKO livers could not be ruled out. Future studies need to focus on determining the extent of hepatic molecular clock disruption and delineate the mechanism of suppression of BMAL1 and CLOCK, the core clock transcription factors in M3LKO mice.

Although hepatic *Mettl3* RNA level varies with circadian time in WT mice,[17] rhythmic changes in METTL3 protein level and its activity (reflected in the m^{6}A landscape) have not been elucidated. Intriguingly, rhythmic expression of several factors, especially the m^{6}A demethylases *Fto* and *AlkBH5*, were recently reported to be up-regulated in the liver at all time points in Bmal1 liver-specific knockout (LKO) mice during the 12-hour day and 12-hour night cycle.[17] As a result, the global m^{6}A/A ratio was elevated and m^{6}A methylation on the *Pparα* transcripts increased in the mutant mice. In contrast, in M3LKO livers m^{6}A/A ratio and m^{6}A enrichment in *Pparα* transcripts decreased without significant changes in *Fto* and *AlkBH5* expression in M3LKO mice (data not shown). This finding suggests that the regulation of the m^{6}A landscape in M3LKO mice is distinct from that of *Bmal1/Arntl* LKO mice.

Role of METTL3 in Liver Cell Cycle and Polyploidy

Highly polyploid hepatocytes of irregular size were noted in M3LKO mice as early as 5 and 10 weeks of age. The presence of both apoptotic and proliferative hepatocytes in *Mettl3*-depleted livers suggests that hepatocytes enter cell cycle to compensate for the damaged cells, and they become polyploid because of impaired cytokinesis. Alternatively, because polyploid hepatocytes have reduced proliferative capacity compared with diploid hepatocytes,[57] M3LKO hepatocytes might be inherently more replicative, like M3LKO ESCs.[14] It is also possible that M3LKO hepatocytes undergo atypical DNA replication, such as endoreplication, characterized by alternating G1-S-G2 phases bypassing mitosis and/or cell division, which generates polyploid nuclei.[58] In the future, it will be important to determine whether polyploidy increases via acytokinetic mitosis (failed or skipped cytokinesis, which occurs during normal postnatal development) or endomitosis (DNA replication without mitosis), which occurs in patients with nonalcoholic fatty liver disease as well as in mouse models of nonalcoholic fatty liver disease and is considered pathologic polyploidy.[59] The G2-M cell cycle regulator WEE1 is reduced in M3LKO livers, and loss of WEE1 has been associated with induced polyploidy,[60,61] suggesting that WEE1 deficiency may promote hepatic polyploidy in M3LKO mice. In addition, it has recently been reported that hepatocyte ploidy varies with circadian rhythm,[47] which suggests hepatocyte DNA replication occurs at a specific time of the day. Because marked differences in ploidy in M3LKO livers compared with WT livers was observed, it will be important to determine whether this difference is associated with disruption of circadian rhythm.

In summary, studies in the M3LKO model indicated that METTL3 exhibits pleotropic function to maintain liver homeostasis by deregulating m^{6}A profile and expression of the liver transcriptome. Therefore, dissecting the molecular mechanisms underlying these functions remains an important task for future studies. It is also important to determine the hepatic m^{6}A profile during prenatal liver development, liver regeneration after toxic liver injury, and carcinogen- or nonalcoholic steatohepatitis−induced hepatocarcinogenesis and the consequence of METTL3 loss of function in these

processes using LKO mice. Another significant goal is to determine the consequences of METTL3 depletion in the hepatocytes as well as other cell types, such as cholangiocytes, Kupffer cells, and stellate cells, in cell type−specific knockout mice.

Acknowledgments

We thank Drs. Jacob Hanna and Federica Accornero for providing *Mettl3*$^{fl/fl}$ mice, Dr. Peng Hu for technical assistance, and Pipasha Biswas for mouse breeding and genotyping.

Supplemental Data

Supplemental material for this article can be found at *http://doi.org/10.1016/j.ajpath.2021.09.005*.

References

1. He PC, He C: m(6) A RNA methylation: from mechanisms to therapeutic potential. EMBO J 2021, 40:e105977
2. Zaccara S, Ries RJ, Jaffrey SR: Reading, writing and erasing mRNA methylation. Nat Rev Mol Cell Biol 2019, 20:608−624
3. Ke S, Alemu EA, Mertens C, Gantman EC, Fak JJ, Mele A, Haripal B, Zucker-Scharff I, Moore MJ, Park CY, Vagbo CB, Kussnierczyk A, Klungland A, Darnell JE Jr, Darnell RB: A majority of m6A residues are in the last exons, allowing the potential for 3' UTR regulation. Genes Dev 2015, 29:2037−2053
4. Ke S, Pandya-Jones A, Saito Y, Fak JJ, Vagbo CB, Geula S, Hanna JH, Black DL, Darnell JE Jr, Darnell RB: m(6)A mRNA modifications are deposited in nascent pre-mRNA and are not required for splicing but do specify cytoplasmic turnover. Genes Dev 2017, 31:990−1006
5. Liu J, Yue Y, Han D, Wang X, Fu Y, Zhang L, Jia G, Yu M, Lu Z, Deng X, Dai Q, Chen W, He C: A METTL3-METTL14 complex mediates mammalian nuclear RNA N6-adenosine methylation. Nat Chem Biol 2014, 10:93−95
6. Dominissini D, Moshitch-Moshkovitz S, Schwartz S, Salmon-Divon M, Ungar L, Osenberg S, Cesarkas K, Jacob-Hirsch J, Amariglio N, Kupiec M, Sorek R, Rechavi G: Topology of the human and mouse m6A RNA methylomes revealed by m6A-seq. Nature 2012, 485:201−206
7. Meyer KD, Jaffrey SR: Rethinking m(6)A readers, writers, and erasers. Annu Rev Cell Dev Biol 2017, 33:319−342
8. Zheng G, Dahl JA, Niu Y, Fedorcsak P, Huang CM, Li CJ, Vagbo CB, Shi Y, Wang WL, Song SH, Lu Z, Bosmans RP, Dai Q, Hao YJ, Yang X, Zhao WM, Tong WM, Wang XJ, Bogdan F, Furu K, Fu Y, Jia G, Zhao X, Liu J, Krokan HE, Klungland A, Yang YG, He C: ALKBH5 is a mammalian RNA demethylase that impacts RNA metabolism and mouse fertility. Mol Cell 2013, 49:18−29
9. Jia G, Fu Y, Zhao X, Dai Q, Zheng G, Yang Y, Yi C, Lindahl T, Pan T, Yang YG, He C: N6-methyladenosine in nuclear RNA is a major substrate of the obesity-associated FTO. Nat Chem Biol 2011, 7:885−887
10. Mauer J, Sindelar M, Despic V, Guez T, Hawley BR, Vasseur JJ, Rentmeister A, Gross SS, Pellizzoni L, Debart F, Goodarzi H, Jaffrey SR: FTO controls reversible m(6)Am RNA methylation during snRNA biogenesis. Nat Chem Biol 2019, 15:340−347
11. Wei J, Liu F, Lu Z, Fei Q, Ai Y, He PC, Shi H, Cui X, Su R, Klungland A, Jia G, Chen J, He C: Differential m(6)A, m(6)Am, and m(1)A demethylation mediated by FTO in the cell nucleus and cytoplasm. Mol Cell 2018, 71:973−985.e5
12. Scuteri A, Sanna S, Chen WM, Uda M, Albai G, Strait J, Najjar S, Nagaraja R, Orru M, Usala G, Dei M, Lai S, Maschio A, Busonero F, Mulas A, Ehret GB, Fink AA, Weder AB, Cooper RS, Galan P, Chakravarti A, Schlessinger D, Cao A, Lakatta E, Abecasis GR: Genome-wide association scan shows genetic variants in the FTO gene are associated with obesity-related traits. PLoS Genet 2007, 3:e115
13. Zhao BS, Roundtree IA, He C: Post-transcriptional gene regulation by mRNA modifications. Nat Rev Mol Cell Biol 2017, 18:31−42
14. Batista PJ, Molinie B, Wang J, Qu K, Zhang J, Li L, Bouley DM, Lujan E, Haddad B, Daneshvar K, Carter AC, Flynn RA, Zhou C, Lim KS, Dedon P, Wernig M, Mullen AC, Xing Y, Giallourakis CC, Chang HY: m(6)A RNA modification controls cell fate transition in mammalian embryonic stem cells. Cell Stem Cell 2014, 15:707−719
15. Geula S, Moshitch-Moshkovitz S, Dominissini D, Mansour AA, Kol N, Salmon-Divon M, Hershkovitz V, Peer E, Mor N, Manor YS, Ben-Haim MS, Eyal E, Yunger S, Pinto Y, Jaitin DA, Viukov S, Rais Y, Krupalnik V, Chomsky E, Zerbib M, Maza I, Rechavi Y, Massarwa R, Hanna S, Amit I, Levanon EY, Amariglio N, Stern-Ginossar N, Novershtern N, Rechavi G, Hanna JH: Stem cells: m6A mRNA methylation facilitates resolution of naive pluripotency toward differentiation. Science 2015, 347:1002−1006
16. Xiang Y, Laurent B, Hsu CH, Nachtergaele S, Lu Z, Sheng W, Xu C, Chen H, Ouyang J, Wang S, Ling D, Hsu PH, Zou L, Jambhekar A, He C, Shi Y: RNA m(6)A methylation regulates the ultraviolet-induced DNA damage response. Nature 2017, 543:573−576
17. Zhong X, Yu J, Frazier K, Weng X, Li Y, Cham CM, Dolan K, Zhu X, Hubert N, Tao Y, Lin F, Martinez-Guryn K, Huang Y, Wang T, Liu J, He C, Chang EB, Leone V: Circadian clock regulation of hepatic lipid metabolism by modulation of m(6)A mRNA methylation. Cell Rep 2018, 25:1816−1828.e4
18. Dorn LE, Lasman L, Chen J, Xu X, Hund TJ, Medvedovic M, Hanna JH, van Berlo JH, Accornero F: The N(6)-methyladenosine mRNA methylase METTL3 controls cardiac homeostasis and hypertrophy. Circulation 2019, 139:533−545
19. Mathiyalagan P, Adamiak M, Mayourian J, Sassi Y, Liang Y, Agarwal N, Jha D, Zhang S, Kohlbrenner E, Chepurko E, Chen J, Trivieri MG, Singh R, Bouchareb R, Fish K, Ishikawa K, Lebeche D, Hajjar RJ, Sahoo S: FTO-dependent N(6)-methyladenosine regulates cardiac function during remodeling and repair. Circulation 2019, 139:518−532
20. Panneerdoss S, Eedunuri VK, Yadav P, Timilsina S, Rajamanickam S, Viswanadhapalli S, Abdelfattah N, Onyeagucha BC, Cui X, Lai Z, Mohammad TA, Gupta YK, Huang THM, Huang Y, Chen Y, Rao MK: Cross-talk among writers, readers, and erasers of m6A regulates cancer growth and progression. Sci Adv 2018, 4:eaar8263
21. Shi H, Wei J, He C: Where, when, and how: context-dependent functions of RNA methylation writers, readers, and erasers. Mol Cell 2019, 74:640−650
22. Cui Q, Shi H, Ye P, Li L, Qu Q, Sun G, Sun G, Lu Z, Huang Y, Yang CG, Riggs AD, He C, Shi Y: m(6)A RNA methylation regulates the self-renewal and tumorigenesis of glioblastoma stem cells. Cell Rep 2017, 18:2622−2634
23. Li Z, Weng H, Su R, Weng X, Zuo Z, Li C, Huang H, Nachtergaele S, Dong L, Hu C, Qin X, Tang L, Wang Y, Hong GM, Huang H, Wang X, Chen P, Gurbuxani S, Arnovitz S, Li Y, Li S, Strong J, Neilly MB, Larson RA, Jiang X, Zhang P, Jin J, He C, Chen J: FTO plays an oncogenic role in acute myeloid leukemia as a

N(6)-methyladenosine RNA demethylase. Cancer Cell 2017, 31: 127−141
24. Zhang S, Zhao BS, Zhou A, Lin K, Zheng S, Lu Z, Chen Y, Sulman EP, Xie K, Bogler O, Majumder S, He C, Huang S: m(6)A demethylase ALKBH5 maintains tumorigenicity of glioblastoma stem-like cells by sustaining FOXM1 expression and cell proliferation program. Cancer Cell 2017, 31:591−606.e6
25. Liu J, Harada BT, He C: Regulation of gene expression by N(6)-methyladenosine in cancer. Trends Cell Biol 2019, 29:487−499
26. Jonkhout N, Tran J, Smith MA, Schonrock N, Mattick JS, Novoa EM: The RNA modification landscape in human disease. RNA 2017, 23:1754−1769
27. Chelmicki T, Roger E, Teissandier A, Dura M, Bonneville L, Rucli S, Dossin F, Fouassier C, Lameiras S, Bourc'his D: m(6)A RNA methylation regulates the fate of endogenous retroviruses. Nature 2021, 591:312−316
28. Xu W, Li J, He C, Wen J, Ma H, Rong B, Diao J, Wang L, Wang J, Wu F, Tan L, Shi YG, Shi Y, Shen H: METTL3 regulates heterochromatin in mouse embryonic stem cells. Nature 2021, 591: 317−321
29. Xie W, Ma LL, Xu YQ, Wang BH, Li SM: METTL3 inhibits hepatic insulin sensitivity via N6-methyladenosine modification of Fasn mRNA and promoting fatty acid metabolism. Biochem Biophys Res Commun 2019, 518:120−126
30. Postic C, Magnuson MA: DNA excision in liver by an albumin-Cre transgene occurs progressively with age. Genesis 2000, 26: 149−150
31. Weisend CM, Kundert JA, Suvorova ES, Prigge JR, Schmidt EE: Cre activity in fetal albCre mouse hepatocytes: utility for developmental studies. Genesis 2009, 47:789−792
32. Rosbash M, Bradley S, Kadener S, Li Y, Luo W, Menet JS, Nagoshi E, Palm K, Schoer R, Shang Y, Tang CH: Transcriptional feedback and definition of the circadian pacemaker in Drosophila and animals. Cold Spring Harb Symp Quant Biol 2007, 72:75−83
33. Hsu SH, Wang B, Kota J, Yu J, Costinean S, Kutay H, Yu L, Bai S, La Perle K, Chivukula RR, Mao H, Wei M, Clark KR, Mendell JR, Caligiuri MA, Jacob ST, Mendell JT, Ghoshal K: Essential metabolic, anti-inflammatory, and anti-tumorigenic functions of miR-122 in liver. J Clin Invest 2012, 122:2871−2883
34. Thoolen B, Maronpot RR, Harada T, Nyska A, Rousseaux C, Nolte T, Malarkey DE, Kaufmann W, Kuttler K, Deschl U, Nakae D, Gregson R, Vinlove MP, Brix AE, Singh B, Belpoggi F, Ward JM: Proliferative and nonproliferative lesions of the rat and mouse hepatobiliary system. Toxicol Pathol 2010, 38:5S−81S
35. Kim D, Paggi JM, Park C, Bennett C, Salzberg SL: Graph-based genome alignment and genotyping with HISAT2 and HISAT-genotype. Nat Biotechnol 2019, 37:907−915
36. Li H, Handsaker B, Wysoker A, Fennell T, Ruan J, Homer N, Marth G, Abecasis G, Durbin R; 1000 Genome Project Data Processing Subgroup: The sequence alignment/map format and SAMtools. Bioinformatics 2009, 25:2078−2079
37. Bray NL, Pimentel H, Melsted P, Pachter L: Near-optimal probabilistic RNA-seq quantification. Nat Biotechnol 2016, 34: 525−527
38. Pimentel H, Bray NL, Puente S, Melsted P, Pachter L: Differential analysis of RNA-seq incorporating quantification uncertainty. Nat Methods 2017, 14:687−690
39. Wilkinson PD, Alencastro F, Delgado ER, Leek MP, Weirich MP, Otero PA, Roy N, Brown WK, Oertel M, Duncan AW: Polyploid hepatocytes facilitate adaptation and regeneration to chronic liver injury. Am J Pathol 2019, 189:1241−1255
40. Nagata T, Redman RS, Lakshman R: Isolation of intact nuclei of high purity from mouse liver. Anal Biochem 2010, 398:178−184
41. Su Q, Bannasch P: Relevance of hepatic preneoplasia for human hepatocarcinogenesis. Toxicol Pathol 2003, 31:126−133
42. Hsu SH, Duncan AW: Pathological polyploidy in liver disease. Hepatology 2015, 62:968−970
43. Hsu SH, Delgado ER, Otero PA, Teng KY, Kutay H, Meehan KM, Moroney JB, Monga JK, Hand NJ, Friedman JR, Ghoshal K, Duncan AW: MicroRNA-122 regulates polyploidization in the murine liver. Hepatology 2016, 64:599−615
44. Fei Q, Zou Z, Roundtree IA, Sun HL, He C: YTHDF2 promotes mitotic entry and is regulated by cell cycle mediators. PLoS Biol 2020, 18:e3000664
45. Masri S, Rigor P, Cervantes M, Ceglia N, Sebastian C, Xiao C, Roqueta-Rivera M, Deng C, Osborne TF, Mostoslavsky R, Baldi P, Sassone-Corsi P: Partitioning circadian transcription by SIRT6 leads to segregated control of cellular metabolism. Cell 2014, 158: 659−672
46. Fustin JM, Doi M, Yamaguchi Y, Hida H, Nishimura S, Yoshida M, Isagawa T, Morioka MS, Kakeya H, Manabe I, Okamura H: RNA-methylation-dependent RNA processing controls the speed of the circadian clock. Cell 2013, 155:793−806
47. Wang J, Mauvoisin D, Martin E, Atger F, Galindo AN, Dayon L, Sizzano F, Palini A, Kussmann M, Waridel P, Quadroni M, Dulic V, Naef F, Gachon F: Nuclear proteomics uncovers diurnal regulatory landscapes in mouse liver. Cell Metab 2017, 25:102−117
48. Schrem H, Klempnauer J, Borlak J: Liver-enriched transcription factors in liver function and development. Part I: the hepatocyte nuclear factor network and liver-specific gene expression. Pharmacol Rev 2002, 54:129−158
49. Schrem H, Klempnauer J, Borlak J: Liver-enriched transcription factors in liver function and development. Part II: the C/EBPs and D site-binding protein in cell cycle control, carcinogenesis, circadian gene regulation, liver regeneration, apoptosis, and liver-specific gene regulation. Pharmacol Rev 2004, 56:291−330
50. Chen M, Wei L, Law CT, Tsang FH, Shen J, Cheng CL, Tsang LH, Ho DW, Chiu DK, Lee JM, Wong CC, Ng IO, Wong CM: RNA N6-methyladenosine methyltransferase-like 3 promotes liver cancer progression through YTHDF2-dependent posttranscriptional silencing of SOCS2. Hepatology 2018, 67:2254−2270
51. Sato K, Marzioni M, Meng F, Francis H, Glaser S, Alpini G: Ductular reaction in liver diseases: pathological mechanisms and translational significances. Hepatology 2019, 69:420−430
52. Chen S, Yang J, Zhang Y, Duan C, Liu Q, Huang Z, Xu Y, Zhou L, Xu G: Ubiquitin-conjugating enzyme UBE2O regulates cellular clock function by promoting the degradation of the transcription factor BMAL1. J Biol Chem 2018, 293:11296−11309
53. Dang F, Sun X, Ma X, Wu R, Zhang D, Chen Y, Xu Q, Wu Y, Liu Y: Insulin post-transcriptionally modulates Bmal1 protein to affect the hepatic circadian clock. Nat Commun 2016, 7:12696
54. Luciano AK, Zhou W, Santana JM, Kyriakides C, Velazquez H, Sessa WC: CLOCK phosphorylation by AKT regulates its nuclear accumulation and circadian gene expression in peripheral tissues. J Biol Chem 2018, 293:9126−9136
55. Sahar S, Zocchi L, Kinoshita C, Borrelli E, Sassone-Corsi P: Regulation of BMAL1 protein stability and circadian function by GSK3beta-mediated phosphorylation. PLoS One 2010, 5:e8561
56. Kondratov RV, Kondratova AA, Gorbacheva VY, Vykhovanets OV, Antoch MP: Early aging and age-related pathologies in mice deficient in BMAL1, the core component of the circadian clock. Genes Dev 2006, 20:1868−1873
57. Wilkinson PD, Delgado ER, Alencastro F, Leek MP, Roy N, Weirich MP, Stahl EC, Otero PA, Chen MI, Brown WK, Duncan AW: The polyploid state restricts hepatocyte proliferation and liver regeneration in mice. Hepatology 2019, 69: 1242−1258
58. Wilkinson PD, Duncan AW: Differential roles for diploid and polyploid hepatocytes in acute and chronic liver injury. Semin Liver Dis 2021, 41:42−49

59. Gentric G, Maillet V, Paradis V, Couton D, L'Hermitte A, Panasyuk G, Fromenty B, Celton-Morizur S, Desdouets C: Oxidative stress promotes pathologic polyploidization in nonalcoholic fatty liver disease. J Clin Invest 2015, 125:981−992
60. Nojima H, Homma H, Onozato Y, Kaida A, Harada H, Miura M: Differential properties of mitosis-associated events following CHK1 and WEE1 inhibitor treatments in human tongue carcinoma cells. Exp Cell Res 2020, 386:111720
61. Vassilopoulos A, Tominaga Y, Kim HS, Lahusen T, Li B, Yu H, Gius D, Deng CX: WEE1 murine deficiency induces hyper-activation of APC/C and results in genomic instability and carcinogenesis. Oncogene 2015, 34:3023−3035